

# Weak Quasielastic Production of Hyperons and Threshold Production of Two Pions.

S. K. Singh\*, M. Sajjad Athar\*, M. Rafi Alam\*, Shikha Chauhan\*, E. Hernández†, J. Nieves\*\*, M. Valverde\*\* and M. J. Vicente Vacas\*\*

\**Department of Physics, Aligarh Muslim University, Aligarh-202 002, India*

†*Grupo de Física Nuclear, Departamento de Física Fundamental e IUFFyM, Universidad de Salamanca, E-37008 Salamanca, Spain.*

\*\**Departamento de Física Teórica and Instituto de Física Corpuscular, Centro Mixto Universidad de Valencia-CSIC, E-46071 Valencia, Spain*

**Abstract.** We have studied quasielastic charged current hyperon production induced by  $\bar{\nu}_\mu$  on free nucleon and the nucleons bound inside the nucleus and the results are presented for several nuclear targets like  $^{40}\text{Ar}$ ,  $^{56}\text{Fe}$  and  $^{208}\text{Pb}$ . The hyperon-nucleon transition form factors are determined from neutrino-nucleon scattering and semileptonic decays of neutron and hyperons using SU(3) symmetry. The nuclear medium effects(NME) due to Fermi motion and final state interaction(FSI) effect due to hyperon-nucleon scattering have been taken into account. Also we have studied two pion production at threshold induced by neutrinos off nucleon targets. The contribution of nucleon, pion, and contact terms are calculated using Lagrangian given by nonlinear  $\sigma$  model. The contribution of the Roper resonance has also been taken into account. The numerical results for the cross sections are presented and compared with the experimental results from ANL and BNL.

**Keywords:** strange particle production, pion production, nuclear medium effects

**PACS:** 13.15+g, 13.75.Ev, 14.20.Jn, 21.60.Jz, 25.30.Pt

## INTRODUCTION

The neutrino oscillation experiments being done using accelerator (anti)neutrino beams in the energy region of few GeV are also providing cross section measurements of various reactions induced by neutrinos and antineutrinos on nuclear targets which are needed for validating various Monte Carlo neutrino event generators. The reported cross sections are available mainly for elastic, quasielastic and single pion production processes on  $^{12}\text{C}$  and  $^{16}\text{O}$  nuclei. The availability of high intensity (anti)neutrino beams in present generation neutrino oscillation experiments has opened up the possibility of cross section measurements of other processes like production of hyperons, strange baryons and multiple pions in the energy region of a few GeV in the experiments being done at MINERvA [1], MINOS [2], NOvA [3], LBNE [4], T2K [5] and MiniBooNE [6]. In the lower energy region relevant for T2K [5] and MicroBooNE [7] experiments, any observation of these processes will help to understand the reaction dynamics of the threshold production of strange mesons and two pions. In view of this scenario, some calculations have been done recently for the production of hyperons [8], kaons [9, 10] and two pions [11].

In this work we present a brief overview of the quasideastic production of hyperons induced by antineutrinos on nucleons and nuclei and charged current two pion production induced by neutrino from nucleon. First, we are going to present the formalism, results and discussion for the quasideastic production of hyperons from nucleons and nuclear targets followed by the formalism of two pion production from nucleons and their results and discussion.

## QUASIELASTIC PRODUCTION OF HYPERONS

### Formalism

The quasideastic production of hyperons induced by antineutrinos has been studied in the past using Cabibbo theory with SU(3) symmetry [12] as well as in quark models [13]. In addition to providing neutrino-nucleus cross section to be used in modeling the MC neutrino event generators, the differential cross sections also provide an opportunity to study nucleon-hyperon transition form factors at high  $Q^2$ , which are available only at low  $Q^2$  through

the analysis of Semileptonic Hyperon Decays(SHD) [14]. An independent determination of these form factors help to test various assumptions made in the analysis of these processes like SU(3) symmetry, G invariance, absence of Flavor Changing Neutral Currents(FCNC),  $\Delta Q = \Delta S$  rule, Conserved Vector Current(CVC) and Partial Conservation of Axial Current(PCAC) hypothesis in the Standard Model(SM) when it is extended to the strangeness sector. Since these hyperons decay primarily through pionic decay modes, they also contribute to the pion production processes induced by antineutrinos, which is dominated by the pion production through  $\Delta$ -excitation. In the low energy region where  $\Delta$ -excitation is inhibited by threshold effects, the Cabibbo suppressed pion production through hyperons( $\Lambda$  and  $\Sigma$ ) production may be important.

We consider the following processes

$$\begin{aligned}\bar{\nu}_\mu(k) + p(p) &\rightarrow \mu^+(k') + \Lambda(p') \\ \bar{\nu}_\mu(k) + p(p) &\rightarrow \mu^+(k') + \Sigma^0(p') \\ \bar{\nu}_\mu(k) + n(p) &\rightarrow \mu^+(k') + \Sigma^-(p'),\end{aligned}\quad (1)$$

where  $k(k')$  and  $p(p')$  are the momenta of initial(final) lepton and nucleon. The differential scattering cross section is given by,

$$d\sigma = \frac{1}{(2\pi)^2} \frac{1}{4E_{\bar{\nu}}M} \delta^4(k+p-k'-p') \frac{d^3k'}{2E_{k'}} \frac{d^3p'}{2E_{p'}} \sum \bar{\sum} |\mathcal{M}|^2, \quad (2)$$

with

$$\mathcal{M} = \frac{G_F}{\sqrt{2}} \sin \theta_c l^\mu J_\mu \quad (3)$$

$$l^\mu = \bar{\nu}(k') \gamma^\mu (1 + \gamma_5) \nu(k) \quad (4)$$

$$J_\mu = \langle Y(p') | V_\mu - A_\mu | N(p) \rangle, \quad (5)$$

where

$$\langle Y(p') | V_\mu | N(p) \rangle = \bar{u}_Y(p') \left[ \gamma_\mu f_1(q^2) + i\sigma_{\mu\nu} \frac{q^\nu}{M+M_Y} f_2(q^2) + \frac{f_3(q^2)}{M+M_Y} q_\mu \right] u_N(p) \quad (6)$$

$$\langle Y(p') | A_\mu | N(p) \rangle = \bar{u}_Y(p') \left[ \gamma_\mu \gamma_5 g_1(q^2) + i\sigma_{\mu\nu} \gamma_5 \frac{q^\nu}{M+M_Y} g_2(q^2) + \frac{g_3(q^2)}{M+M_Y} q_\mu \gamma_5 \right] u_N(p), \quad (7)$$

The form factors  $f_i(q^2)$  and  $g_i(q^2)$  are determined using T invariance, G invariance, SU(3) symmetry (symmetry properties of weak currents) like CVC and PCAC hypothesis. These symmetry considerations yield [12]:

1.  $f_i(q^2)$  and  $g_i(q^2)$  as real quantities
2.  $f_3(q^2) = g_2(q^2) = 0$
3.  $g_3(q^2) = \frac{m_\pi}{m_\pi^2 - q^2} g_1(q^2)$
4.  $f_{i=1,2}^{p \rightarrow \Sigma^0} \left( g_{i=1,2}^{p \rightarrow \Sigma^0} \right) = \frac{1}{\sqrt{2}} f_{i=1,2}^{p \rightarrow \Sigma^-} \left( g_{i=1,2}^{p \rightarrow \Sigma^-} \right)$
5. The form factors,  $f_{1,2}(q^2) = \frac{1}{\sqrt{2}} (f_{1,2}^p(q^2) + 2f_{1,2}^n(q^2))$  and  $f_{1,2}(q^2) = -\sqrt{\frac{3}{2}} f_{1,2}^p(q^2)$  respectively for transitions  $p \rightarrow \Sigma^0$  and  $p \rightarrow \Lambda$ . Similarly  $g_1(q^2)$  is  $\frac{1}{\sqrt{2}} \frac{D-F}{D+F} g_A(q^2)$  for  $p \rightarrow \Sigma^0$  and is  $-\frac{D+3F}{\sqrt{6}(D+F)} g_A(q^2)$  for  $p \rightarrow \Lambda$  transitions. We have used  $D = 0.804$  and  $F = 0.463$  and the following  $q^2$  dependence of the electroproduction and weak form factors [15]:

$$f_1^{p,n}(q^2) = \frac{1}{1 - \frac{q^2}{4M^2}} \left[ G_E^{p,n}(q^2) - \frac{q^2}{4M^2} G_M^{p,n}(q^2) \right], \quad f_2^{p,n}(q^2) = \frac{1}{1 - \frac{q^2}{4M^2}} \left[ G_M^{p,n}(q^2) - G_E^{p,n}(q^2) \right]. \quad (8)$$

The Sach's form factors  $G_E^{p,n}(q^2)$  and  $G_M^{p,n}(q^2)$  are parameterized as

$$\begin{aligned}G_E^p(q^2) &= \left( 1 - \frac{q^2}{M_V^2} \right)^{-2}, & G_M^p(q^2) &= (1 + \mu_p) G_E^p(q^2), \\ G_M^n(q^2) &= \mu_n G_E^p(q^2), & G_E^n(q^2) &= \frac{q^2}{4M^2} \mu_n G_E^p(q^2) \xi_n;\end{aligned}\quad (9)$$

The numerical values of various parameters are taken as

$$\begin{aligned}\xi_n &= \frac{1}{1 - \lambda_n \frac{q^2}{4M_A^2}}, & \mu_p &= 1.792847, \\ \mu_n &= -1.913043, & M_V &= 0.84 \text{ GeV} \text{ and } \lambda_n = 5.6\end{aligned}\quad (10)$$

For  $g_A(q^2)$  a dipole form has been taken i.e.  $g_A(q^2) = g_A(0) \left(1 - \frac{q^2}{M_A^2}\right)^{-2}$  with  $g_A(0) = 1.267$  and the axial dipole mass  $M_A = 1 \text{ GeV}$ .

## Nuclear Medium Effects and Final State Interaction Effects

When these reactions take place on bound nucleons in nuclear medium, Fermi motion and Pauli Blocking effects of nucleons are to be considered. In the final state after hyperons are produced, they may undergo strong interaction scattering processes through charge exchange ( $\Sigma^- p \rightarrow \Lambda n$ ,  $\Lambda p \rightarrow \Sigma^+ n$ , etc.) and inelastic ( $\Lambda N \rightarrow \Sigma^0 N$ ,  $YN \rightarrow Y'N'$ ) reactions like changing the relative yield of  $\Sigma^0$ ,  $\Sigma^-$  and  $\Lambda$  produced in the initial reactions shown in Eq. 1. In a special case,  $\Sigma^+$  will appear as a result of final state interaction which are initially not produced through  $\bar{\nu}_\mu N \rightarrow \mu^+ N$  reaction due to  $\Delta Q = \Delta S$  rule.

The nuclear medium effects are calculated in a relativistic Fermi Gas model using local density approximation and the nuclear cross section is written as

$$\frac{d\sigma}{d\Omega_l dE_l} = 2 \int d^3r \int \frac{d^3p}{(2\pi)^3} n_N(p, r) \left[ \frac{d\sigma}{d\Omega_l dE_l} \right]_{free} \quad (11)$$

where  $n_N(p, r)$  is local occupation number of the initial nucleon of momentum  $p$  and is 1 for  $p < p_{F_N}$  and 0 otherwise with

$$p_{F_N} = [3\pi^2 \rho_N(r)]^{1/3} \quad \text{for } N = n, p \quad (12)$$

The final state interaction of hyperon-nucleon system is calculated in a Monte Carlo simulation approach. In this approach an initial hyperon produced at a position  $\mathbf{r}$  within the nucleus which interacts with a nucleon to produce a new hyperon-nucleon state  $f = Y_f N_f$ , within a distance  $l$  with probability  $P_Y dl$  where  $P_Y$  is the probability per unit length given by

$$P_Y = \sigma_{Y+n \rightarrow f}(E) \rho_n(r) + \sigma_{Y+p \rightarrow f}(E) \rho_p(r), \quad (13)$$

where  $\rho_n(r)$  ( $\rho_p(r)$ ) is the local density of neutron (proton) in the nucleus and  $\sigma$  is the cross section for  $YN \rightarrow f$  process. Now a particular channel  $f$  is selected. For the selected channel  $f$ , a hyperon-nucleon state is chosen by randomly selecting the momentum of initial nucleon consistent with Pauli blocking. A random scattering angle is generated using isotropic cross section for the hyperon-nucleon scattering cross section  $\sigma$ , which then determines momentum (energy) of final hyperon and nucleon. If the momentum of final nucleon is above Fermi momentum, a new final state of  $YN$  system is obtained. This process is continued until the hyperon gets out of the nucleus. All the channels i.e.  $Y + n \rightarrow Y_f + N_f$  and  $Y + p \rightarrow Y_f + N_f$  leading to a final state  $f$  are considered. These hyperons decay into pions through the processes.

$$\Sigma^0(\Lambda^0) \rightarrow p\pi^-, n\pi^0, \quad \Sigma^+ \rightarrow p\pi^0, n\pi^+, \quad \Sigma^- \rightarrow n\pi^- \quad (14)$$

In the final state, a  $\mu^+$  will be accompanied either by a  $\pi^0$  or  $\pi^-$  and rarely by a  $\pi^+$  which will be produced as a result of the final state interaction in the nucleus. Note that it can also be produced as final state interaction effect when  $\pi^0 p \rightarrow \pi^+ n$  reaction takes place.

## Results

In Fig. 1, we have presented the results for the total cross section for  $\bar{\nu}_\mu + p \rightarrow \mu^+ + \Lambda$  reaction for free nucleons and compared them with the experimental results [16, 17, 18, 19, 20, 21]. We have also compared our results with the other theoretical results in quark model obtained by Wu et. al. [13] and Finjord et. al. [22] and in Cabibbo model

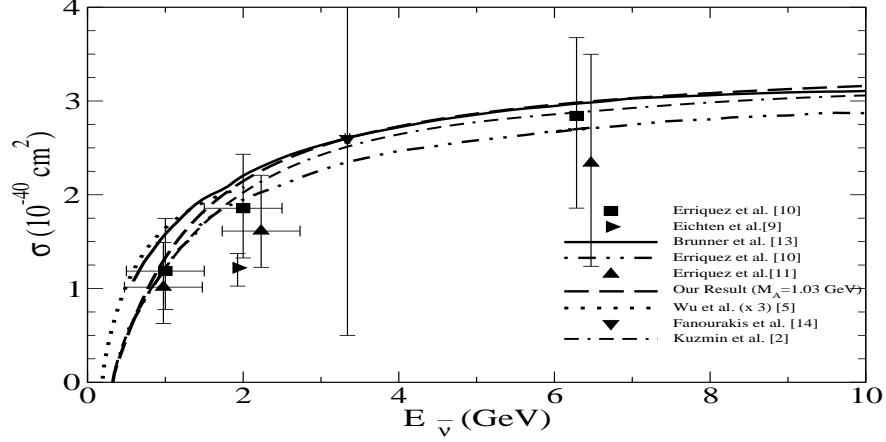


**FIGURE 1.**  $\sigma$  vs  $E_{\bar{\nu}_\mu}$ , for  $\bar{\nu}_\mu + p \rightarrow \mu^+ + \Lambda$  process. Experimental results (triangle right [16], square [17], triangle up [18], circle [19]), triangle down ( $\sigma = 2.6^{+5.9}_{-2.1} \times 10^{-40} \text{cm}^2$ ) [20] are shown with error bars. Theoretical curves are of Erriquez et al. [17](dashed-double dotted line), Brunner et al. [19](dashed line), and Kuzmin and Naumov [21](double dashed-dotted line) obtained using Cabibbo theory with axial vector dipole mass as 1 GeV, 1.1 GeV and 0.999GeV respectively, while the results of Wu et al. [13](dotted line) and Finjord and Ravndal [22](dashed dotted line) are obtained using quark model. The results of present calculation are shown with solid line. Notice that we have multiplied the results of Wu et al. [13] by 3 to plot on the same scale.

by Kuzmin et. al. [21]. We see that the most recent results in quark model by Wu et. al. [13] underestimate the cross sections. The theoretical results presented in Fig. 1 do not include nuclear medium effects while the experimental results are on nuclear targets. Obviously experimental data with better statistics are needed to study nuclear medium effects. However, Cabibbo theory with  $SU(3)$  symmetry seems to work well for explaining the present results on  $\bar{\nu}_\mu p \rightarrow \mu^+ \Lambda$ . In Fig. 2, we show the results for  $\bar{\nu}_\mu p \rightarrow \mu^+ \Sigma^0$  where new data are needed to draw any conclusion. For completeness we present the results for  $\bar{\nu}_\mu p \rightarrow \mu^+ \Lambda$  in  $^{40}\text{Ar}$ ,  $^{56}\text{Fe}$  and  $^{208}\text{Pb}$  in Fig. 3 where we also show the effect of final state interactions.

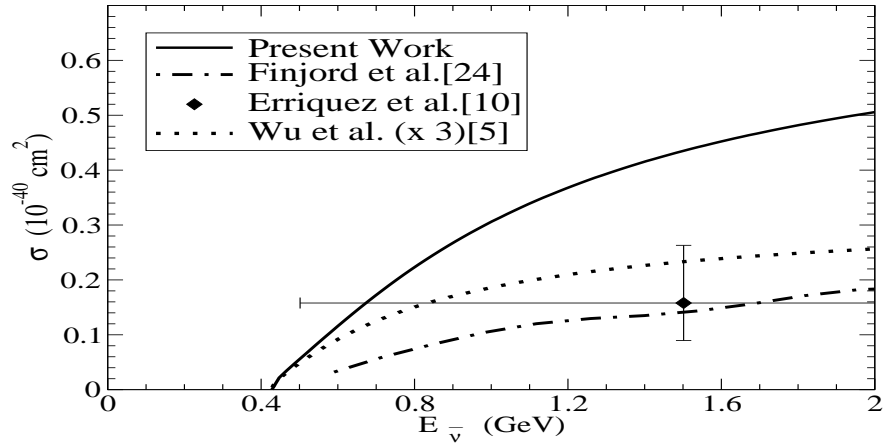


**FIGURE 2.**  $\sigma$  vs  $E_{\bar{\nu}_\mu}$ , for  $\bar{\nu}_\mu + p \rightarrow \mu^+ + \Sigma^0$  process. Experimental points is taken from [17]. Present results are shown with solid line. Also the results of Wu et al. [13](dotted line) and Finjord and Ravndal [22](dashed dotted line) have been presented. Notice that we have multiplied the results of Wu et al. [13] by 3 to plot on the same scale.

In Fig. 4, we present the results for  $\left\langle \frac{d\sigma}{dQ^2} \right\rangle$  in  $^{40}\text{Ar}$  averaged over the MiniBooNE antineutrino spectrum [6] and for  $^{56}\text{Fe}$  and  $^{208}\text{Pb}$  averaged over the MINERvA antineutrino spectrum [23]. It should be noted that lepton energy spectrum i.e.  $\left\langle \frac{d\sigma}{dQ^2} \right\rangle$  can be easily obtained from the  $Q^2$  distribution in each case. The details are given in Ref. [15].

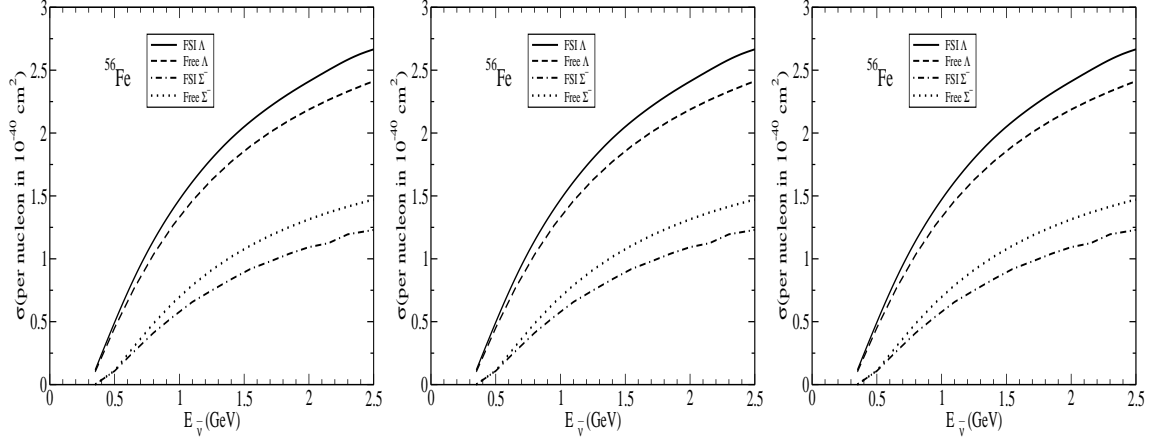


FIGURE 3.  $\sigma$  vs  $E_{\bar{\nu}_\mu}$  for  $^{40}\text{Ar}$ ,  $^{56}\text{Fe}$  and  $^{208}\text{Pb}$  nuclei.

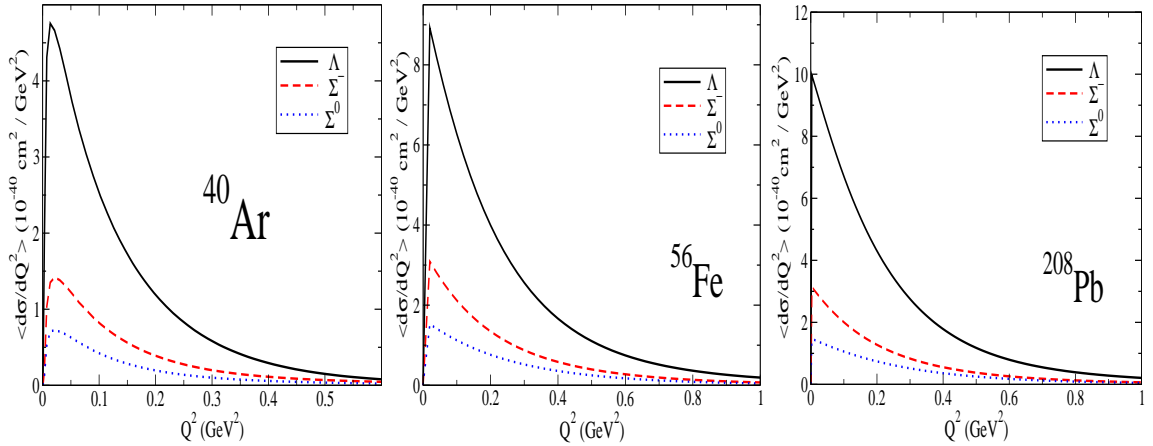


FIGURE 4.  $\langle \frac{d\sigma}{dQ^2} \rangle$  vs  $Q^2$  (Left panel) in  $^{12}\text{C}$ ,  $^{56}\text{Fe}$  and  $^{208}\text{Pb}$  nuclear targets obtained by averaging  $Q^2$ -distribution over the MINERvA [23] flux for the reaction given in Eq. 1. The results are presented with nuclear medium and final state interaction effects.

## THRESHOLD PRODUCTION OF TWO PIONS

Two pion production is the threshold process of inelastic reactions beyond single pion production. Experimental observation of following processes on nucleon targets

$$\nu_\mu p \rightarrow \mu^- p \pi^+ \pi^0 \quad (15)$$

$$\nu_\mu p \rightarrow \mu^- n \pi^+ \pi^+ \quad (16)$$

$$\nu_\mu n \rightarrow \mu^- p \pi^+ \pi^- \quad (17)$$

have been reported at ANL [24] and BNL [25] experiments. To the best of our knowledge no theoretical calculation has been reported in literature except in the threshold region [11, 26]. These calculations make use of an effective chiral Lagrangian to describe the interaction of weak currents with pions and nucleons. It seems that the resonance contribution is as important as the contribution of nucleons and pions (including the contact term) even in the threshold region. It may turn out that the  $2\pi$  production is dominated by processes in which a pion is produced along with a  $\Delta$  in the intermediate state giving rise to another pion as happens in the electroproduction [27, 28]. Calculations of two pion production in an intermediate  $\Delta$  dominance model will be very useful in analyzing the existing data from ANL [24] and BNL [29] experiments on two pion production and data to be obtained in future from the experiments looking for neutrino oscillation.

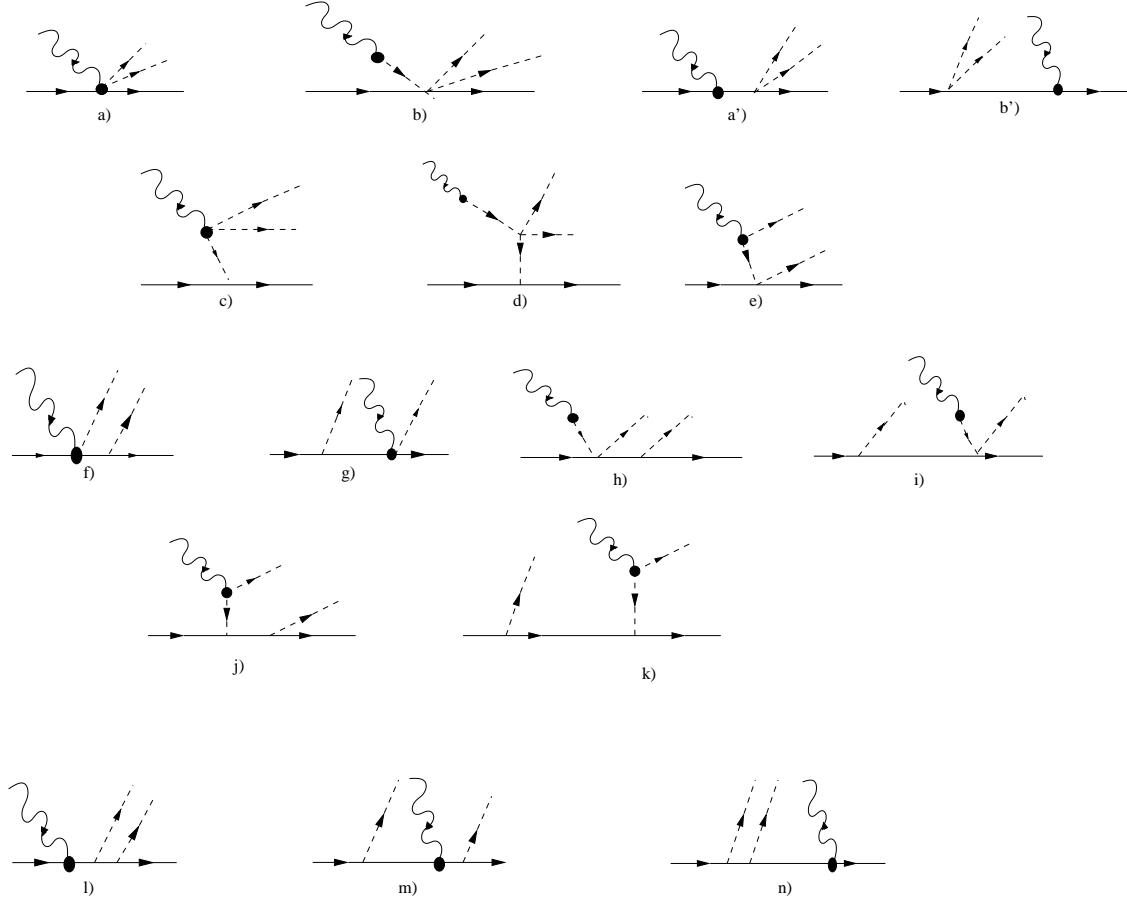


**FIGURE 5.** Nucleon pole, pion pole and contact terms contributing to  $2\pi$  production.

In this work, we report the calculation of weak charged current production of two pions in threshold region. We use a nonlinear chiral Lagrangian model which has been extensively used to study the single pion production [30]. The Lagrangian describes the interaction of pions and nucleons and generates the weak vector and axial vector current under a  $SU(2) \times SU(2)$  transformation which interacts with  $W^\pm/Z$  boson as described by the Standard Model. The effective Lagrangian is given as

$$\begin{aligned} \mathcal{L}_{\text{int}}^\sigma &= \frac{g_A}{f_\pi} \bar{\Psi} \gamma^\mu \gamma_5 \frac{\vec{\tau}}{2} (\partial_\mu \vec{\phi}) \Psi - \frac{1}{4f_\pi^2} \bar{\Psi} \gamma_\mu \vec{\tau} (\vec{\phi} \times \partial^\mu \vec{\phi}) \Psi - \frac{1}{6f_\pi^2} (\vec{\phi}^2 \partial_\mu \vec{\phi} \partial^\mu \vec{\phi} - (\vec{\phi} \partial_\mu \vec{\phi})(\vec{\phi} \partial^\mu \vec{\phi})) + \frac{m_\pi^2}{24f_\pi^2} (\vec{\phi}^2)^2 \\ &\quad - \frac{g_A}{6f_\pi^3} \bar{\Psi} \gamma^\mu \gamma_5 \left[ \vec{\phi}^2 \frac{\vec{\tau}}{2} \partial_\mu \vec{\phi} - (\vec{\phi} \partial_\mu \vec{\phi}) \frac{\vec{\tau}}{2} \vec{\phi} \right] \Psi, \end{aligned} \quad (18)$$

where  $\Psi = \begin{pmatrix} p \\ n \end{pmatrix}$  is the nucleon field,  $\vec{\phi}$  is the isovector pion field,  $\vec{\tau}$  are the Pauli matrices and  $f_\pi = 93$  MeV is the pion decay constant. The vector ( $V_\mu$ ) and axial vector ( $A_\mu$ ) currents generated by this Lagrangian under chiral transformation are given by

$$\vec{V}^\mu = \underbrace{\vec{\phi} \times \partial^\mu \vec{\phi}}_{\vec{V}_a^\mu} + \underbrace{\bar{\Psi} \gamma^\mu \frac{\vec{\tau}}{2} \Psi}_{\vec{V}_b^\mu} + \underbrace{\frac{g_A}{2f_\pi} \bar{\Psi} \gamma^\mu \gamma_5 (\vec{\phi} \times \vec{\tau}) \Psi}_{\vec{V}_c^\mu} - \frac{1}{4f_\pi^2} \bar{\Psi} \gamma^\mu \left[ \vec{\tau} \vec{\phi}^2 - \vec{\phi} (\vec{\tau} \cdot \vec{\phi}) \right] \Psi - \frac{\vec{\phi}^2}{3f_\pi^2} (\vec{\phi} \times \partial^\mu \vec{\phi}) + \mathcal{O}\left(\frac{1}{f_\pi^3}\right) \quad (19)$$

$$\begin{aligned}
\vec{A}^\mu &= \underbrace{f_\pi \partial^\mu \vec{\phi}}_{\vec{A}_a^\mu} + \underbrace{g_A \bar{\Psi} \gamma^\mu \gamma_5 \frac{\vec{\tau}}{2} \Psi}_{\vec{A}_b^\mu} + \underbrace{\frac{1}{2f_\pi} \bar{\Psi} \gamma^\mu (\vec{\phi} \times \vec{\tau}) \Psi}_{\vec{A}_c^\mu} \\
&+ \underbrace{\frac{2}{3f_\pi} [\vec{\phi}(\vec{\phi} \cdot \partial^\mu \vec{\phi}) - \vec{\phi}^2 \partial^\mu \vec{\phi}] - \frac{g_A}{4f_\pi^2} \bar{\Psi} \gamma^\mu \gamma_5 [\vec{\tau} \vec{\phi}^2 - \vec{\phi}(\vec{\tau} \cdot \vec{\phi})]}_{\vec{A}_d^\mu} \Psi + \mathcal{O}\left(\frac{1}{f_\pi^3}\right)
\end{aligned} \tag{20}$$

These currents couple to  $W^\pm(Z)$  boson for charged current( neutral current) interaction with nucleon and pion as described in the Standard Model. Various terms in  $V_\mu$  and  $A_\mu$  describe the vector and axial vector couplings for  $WNN$ ,  $WN\pi$   $WNN\pi$  etc. vertices. And the matrix elements for various Feynman diagrams can be calculated for  $\bar{\nu}N \rightarrow \mu^- \pi\pi N$  process using the rules of covariant perturbation theory. Using these currents given in Eqs. 19 and 20 we obtain following 16 diagrams for  $2\pi$  productions shown in Fig. 5, for which the matrix element can be explicitly written using  $W^+ + N \rightarrow N$ ,  $W^+ + N \rightarrow N\pi$ ,  $W^+ + N \rightarrow N\pi\pi$  and  $W^+ \pi \rightarrow \pi$  vertices from Eqs. 19 and 20. The  $\pi NN$  and  $\pi\pi NN$  etc. couplings are derived from Eq. 18. With these matrix elements for the hadronic transition current  $J_\mu$ , the matrix element for the process  $\nu_\mu(k) + N(p) \rightarrow \mu^-(k') + \pi(k_{\pi_1}) + \pi(k_{\pi_2}) + N(p')$  is written as

$$\mathcal{M} = \frac{G_F}{\sqrt{2}} \cos \theta_c l^\mu J_\mu, \tag{21}$$

where

$$l^\mu = \bar{u}(k') \gamma^\mu (1 - \gamma^5) u(k) \tag{22}$$

and

$$J_\mu = \langle N^*(p') \pi(k_{\pi_1}) \pi(k_{\pi_2}) | j_\mu | N(p) \rangle \tag{23}$$

The present formalism gives the correct form of the nucleon vector ( $V_b^\mu$ ) and axial vector ( $A_b^\mu$ ) currents which couple to the  $W^\pm$  boson but go with a point coupling for the  $WNN$  vertex. The form factors are phenomenologically introduced at this vertex which are consistent with electron proton and neutrino nucleon scattering. The following forms are used for the matrix element for  $V_b^\mu$  and  $A_b^\mu$  currents

$$V_b^\mu(q) = 2 \times \left( f_1^V(q^2) \gamma^\mu + i \mu_V \frac{f_2^V(q^2)}{2M} \sigma^{\mu\nu} q_\nu \right), \quad A_b^\mu(q) = g_1(q^2) \times \left( \gamma^\mu \gamma_5 + \frac{q}{m_\pi^2 - q^2} q^\mu \gamma_5 \right). \tag{24}$$

with  $f_{1,2}^V(q^2) = f_{1,2}^p(q^2) - f_{1,2}^n(q^2)$  where the vector form factors  $f_{1,2}^{p,n}$  and the axial vector form factor  $g_1(q^2)$  are given by Eq. 8.

The explicit expressions for the matrix elements of 16 Feynman diagrams shown in Fig. 5 contributing to  $J_\mu$  are given in Ref. [11]. The cross section is then expressed as

$$\frac{d\sigma_{\nu l}}{d\Omega(\hat{k}') dE'} = \frac{G^2}{4\pi^2} \frac{|\vec{k}'|}{|\vec{k}|} L_{\mu\sigma} (W_{CC2\pi}^{\mu\sigma}) \tag{25}$$

with

$$\begin{aligned}
L_{\mu\sigma} &= (L_s)_{\mu\sigma} \pm i(L_a)_{\mu\sigma} = k'_\mu k_\sigma + k'_\sigma k_\mu - g_{\mu\sigma} k \cdot k' \pm i \epsilon_{\mu\sigma\alpha\beta} k'^\alpha k^\beta \\
W_{CC2\pi}^{\mu\sigma} &= \sum_{\text{spins}} \int \frac{d^3 p'}{(2\pi)^3} \frac{M}{E_N} \frac{d^3 k_{\pi_1}}{(2\pi)^3} \frac{1}{2E_{\pi_1}} \frac{d^3 k_{\pi_2}}{(2\pi)^3} \frac{1}{2E_{\pi_2}} (2\pi)^3 \delta^4(p' + k_{\pi_1} + k_{\pi_2} - q - p) \\
&\langle N' \pi_1 \pi_2 | j_{cc+}^\mu(0) | N \rangle \langle N' \pi_1 \pi_2 | j_{cc+}^\sigma(0) | N \rangle^*
\end{aligned} \tag{26}$$

## CONTRIBUTION OF $N^*(1440)$ RESONANCE

The Roper  $N^*(1440)$  is the lowest lying resonance with significant coupling to two pion decay mode in  $S$  state and is expected to contribute in the threshold region. The  $N^* \rightarrow N\pi\pi$  coupling has been studied in  $\pi N \rightarrow \pi\pi N$



**FIGURE 6.** Direct (left) and crossed (right) Roper excitation contributions to  $2\pi$  production.

and  $NN \rightarrow NN\pi\pi$  reactions [31] where  $N^*$  contribution found to be important. The  $N^* \rightarrow N\pi\pi$  is described by the Lagrangian

$$\mathcal{L}_{N^*N\pi\pi} = -c_1^* \frac{m_\pi^2}{f_\pi^2} \bar{\psi}_{N^*} \vec{\phi}^2 \Psi + c_2^* \frac{1}{f_\pi^2} \bar{\psi}_{N^*} (\vec{\tau} \partial_0 \vec{\phi}) (\vec{\tau} \partial_0 \vec{\phi}) \Psi + h.c., \quad (28)$$

with  $c_1^* = -7.27 \text{ GeV}^{-1}$ ,  $c_2^* = 0 \text{ GeV}^{-1}$  [31].

The Feynman diagram for  $\nu_\mu N \rightarrow \mu^- N\pi\pi$  through  $N^*$  excitation is shown in Fig. 6, for which the matrix element is written as

$$\mathcal{M} = 2g^* \bar{u}(p') [S_R(p+q) J_R^\mu(q) + \tilde{J}_R^\mu(q) S_R(p'-q)] u(p); \quad \tilde{J}_R^\mu = \gamma^0 J_R^{\mu\dagger} \gamma^0 \quad (29)$$

where  $S_R$  is the propagator for Roper resonance

$$S_R(p_*) = \frac{\not{p}_* + M_R}{p_*^2 - M_R^2 + i(M_R + W)\Gamma_{\text{tot}}(W)/2}. \quad (30)$$

and

$$J_R^\mu = \frac{F_1^{V^*}(q^2)}{\mu^2} (q^\mu \not{q} - q^2 \gamma^\mu) + i \frac{F_2^{V^*}(q^2)}{\mu} \sigma^{\mu\nu} q_\nu - G_A \gamma^\mu \gamma_5 - \frac{G_P}{\mu} q^\mu \not{q} \gamma_5 - \frac{G_T}{\mu} \sigma^{\mu\nu} q_\nu \gamma_5 \quad (31)$$

with  $\mu = M_N + M_R$ ;  $M_N$  and  $M_R$  are respectively the mass of nucleon and Roper resonance and  $g^* = -c_1^* \frac{m_\pi^2}{f_\pi^2}$ .

The axial vector form factor  $G_P$  is obtained using PCAC hypothesis as

$$G_P(q^2) = \frac{M_N + M_R}{m_\pi^2 - q^2} G_A(q^2). \quad (32)$$

and  $G_A(0)$  is given by Goldberger-Treiman relation

$$G_A(0) = 2f_\pi \frac{\tilde{f}}{m_\pi} = 0.63 \quad (33)$$

with  $\tilde{f}$  is strength of  $N^*N\pi$  coupling determined by the  $N^* \rightarrow N\pi$  decay width  $\Gamma$

$$\Gamma = \frac{3}{2\pi} \left( \frac{\tilde{f}}{m_\pi} \right)^2 \frac{M}{W} |q_{\text{cm}}|^3, \quad (34)$$

with  $W$  as center of mass energy of  $\pi N$  state and  $|q_{\text{cm}}|$  is the center of mass momentum. With  $\Gamma = 350 \text{ MeV}$ , we obtain  $\tilde{f} = 0.48$ . For  $G_A(q^2)$ ,  $q^2$  dependence is assumed to be of dipole form i.e.

$$G_A(q^2) = \frac{G_A(0)}{(1 - q^2/M_A^2)^2}, \quad (35)$$

with  $M_A = 1 \text{ GeV}$ . The isovector vector form factors  $F_1^{V^*} = F_{1p}^* - F_{1n}^*$  and  $F_2^{V^*} = F_{2p}^* - F_{2n}^*$  are determined from the helicity amplitudes defined as

$$A_{1/2}^N = \sqrt{\frac{2\pi\alpha}{k_R}} \langle N^* \uparrow | \sum_{\text{pol}} \varepsilon \cdot j_{\text{e.m.}}(0) | N \downarrow \rangle \xi S_{1/2}^N = \sqrt{\frac{2\pi\alpha}{k_R}} \frac{|\vec{q}|}{\sqrt{-q^2}} \langle N^* \uparrow | \sum_{\text{pol}} \varepsilon \cdot j_{\text{e.m.}}(0) | N \uparrow \rangle \xi, \quad (36)$$



where the polarization vectors are given by

$$\varepsilon^\pm = \frac{1}{\sqrt{2}}(0, \mp 1, -i, 0), \quad (37)$$

and for a photon of momentum  $q$  moving along the positive z-axis

$$\varepsilon^0 = \frac{1}{\sqrt{-q^2}}(|\vec{q}|, 0, 0, q^0). \quad (38)$$

with  $N$  for proton or neutron,  $\alpha = 1/137$ ,  $q$  is the momentum of the virtual photon,  $k_R = (W^2 - M^2)/2W$  and  $W$  is the center of mass energy of the Roper.

The EM  $\gamma N \rightarrow N^*$  current is written as

$$\langle N^*; \vec{p}_* = \vec{p} + \vec{q} | j_{\text{e.m.}}^\alpha(0) | N; \vec{p} \rangle = \bar{u}_*(\vec{p}_*) \left[ \frac{F_1^{N^*}(q^2)}{\mu^2} (q^\alpha \not{q} - q^2 \gamma^\alpha) + i \frac{F_2^{N^*}(q^2)}{\mu} \sigma^{\alpha\nu} q_\nu \right] u(\vec{p}). \quad (39)$$

Using Eqs. 36-39, we obtain the following relations:

$$A_{1/2}^N = |\vec{q}| g(q^2) \left[ \frac{F_2^{N^*}}{\mu} - \frac{q^2}{W+M} \frac{F_1^{N^*}}{\mu^2} \right] \quad (40)$$

$$S_{1/2}^N = \frac{1}{\sqrt{2}} |\vec{q}|^2 g(q^2) \left[ \frac{F_1^{N^*}}{\mu^2} - \frac{F_2^{N^*}}{\mu} \frac{1}{W+M} \right], \quad (41)$$

with

$$g(q^2) = \sqrt{\frac{8\pi\alpha(W+M)W^2}{M(W-M)((W+M)^2 - q^2)}}. \quad (42)$$

Inverting Eqs. 40 and 41 to obtain  $F_1^{N^*}$  and  $F_2^{N^*}$  in terms of  $A_{1/2}^N$  and  $S_{1/2}^N$  and using quark model predictions of  $A_{1/2}^n = -2/3A_{1/2}^p$  and  $S_{1/2}^n = 0$  we obtain

$$F_1^{V^*} = \frac{F_1^{p^*}((M+W)^2 - 5q^2/3) + 2/3F_2^{p^*}(M+W)\mu}{(M+W)^2 - q^2} \quad (43)$$

$$F_2^{V^*} = \frac{F_2^{p^*}(5(M+W)^2 - 3q^2)\mu - 2F_1^{p^*}q^2(M+W)}{3((M+W)^2 - q^2)\mu}. \quad (44)$$

The  $q^2$  dependence of  $F_1^{p^*}$  and  $F_2^{p^*}$  have been obtained by fitting the data on proton-Roper electromagnetic transition form factors to the experimental results in helicity amplitudes and their forms are obtained as

$$F_1^{p^*}(q^2) = \frac{g_1^p/D_V}{1 - q^2/X_1 M_V^2} \quad F_2^{p^*}(q^2) = \frac{g_2^p}{D_V} \left( 1 - X_2 \ln \left( 1 - \frac{q^2}{1 \text{ GeV}^2} \right) \right) \quad (45)$$

## RESULTS

We present numerical results for the different channels using the matrix elements corresponding to various Feynman diagrams shown in Fig. 5 and Fig. 6. All the coupling constants and form factors are fixed as described in the text through Eqs 18-20. The relative phases between different diagrams in Fig. 5 are fixed by the Lagrangian itself.

In the case of resonance contribution the sign of  $N^*N\pi$  coupling is taken to be same as  $NN\pi$  coupling. The axial form factors are used as given in Eqs 31-33. For vector form factors  $F_1^{V^*}$  and  $F_2^{V^*}$  we have considered four cases i.e. FF1, FF2, FF3, FF4 as follows.

FF1: Our fit of helicity amplitude given by MAID [11]

FF2: Form Factors as determined in the quark model of Meyer et al. [32]

FF3: Parameters given by Lalakulich et al. [33]

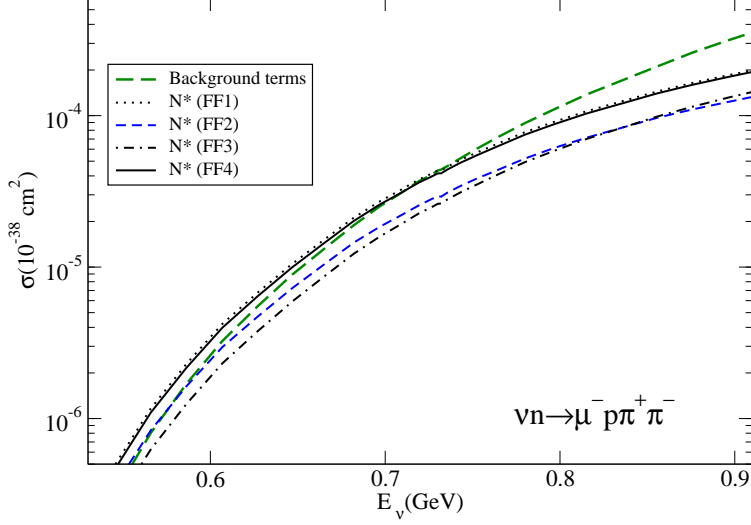


**FIGURE 7.** Cross section for the  $\nu_{\mu}n \rightarrow \mu^{-}p\pi^{+}\pi^{-}$  reaction as a function of the neutrino energy. The interference between background and the  $N^{*}$  contribution is not shown. See text for details.

#### FF4: MAID analysis of helicity amplitudes [34]

In Fig. 7, we present the results for the cross section for the process  $\nu_{\mu}n \rightarrow \mu^{-}p\pi^{+}\pi^{-}$ . We show separately the contribution of background terms (pion and nucleon, including the contact terms) and Roper resonance. We see that at lower energies the contribution of Roper is comparable to the background terms and can be more or less than background contribution depending upon the form factors used. The resonance contribution is sensitive to  $F_2^{V*}(q^2)$ . At higher energies  $E_{\nu} > 0.7\text{GeV}$ , background terms dominate. In Fig. 8, we present the results for this process with experimental results [29, 35] in kinematical region restricted by

$$q_{\pi}^2 \leq ((1 + \eta/2)m_{\pi})^2, \quad (46)$$

$$p \cdot q_{\pi} \leq (M + (1 + \eta)m_{\pi})^2 - M^2 - m_{\pi}^2 \quad (47)$$

$$p' \cdot q_{\pi} \leq (M + (1 + \eta)m_{\pi})^2 - M^2 - m_{\pi}^2, \quad (48)$$

Obviously our model underestimates the experimental results indicating the contribution of other resonances or even the presence of intermediate  $\Delta\pi$  state in this kinematics region.

In Fig. 9, we present the results for  $\nu_{\mu}p \rightarrow \mu^{-}n\pi^{+}\pi^{+}$  and compared them with the experimental results [35]. Here again, our results are lower than the experimental results in this channel. It should be noted that while our results underestimate the experimental results in all these channels, they are larger than the results obtained by Adjei et. al. [26]. In view of this an improved calculation is highly desired for weak pion production in threshold region as well as at higher neutrino energies. In Fig. 10 we present our prediction for the cross section for other channels like:

$$\nu_{\mu}p \rightarrow \mu^{-}p\pi^{+}\pi^0 \quad (49)$$

$$\nu_{\mu}p \rightarrow \mu^{-}n\pi^{+}\pi^{+} \quad (50)$$

$$\nu_{\mu}n \rightarrow \mu^{-}n\pi^{+}\pi^0 \quad (51)$$

$$\nu_{\mu}n \rightarrow \mu^{-}p\pi^0\pi^0 \quad (52)$$

## CONCLUSION

In this work we have presented a review of the theoretical calculation of reactions for the production of leptons due to quasielastic production of hyperons  $\bar{\nu}_{\mu}N \rightarrow \mu^{+}Y$  and two pion production  $\nu_{\mu}N \rightarrow \mu^{-}\pi\pi'N$ . These are the lowest threshold processes beyond the single pion production and may be seen in the present generation of neutrino

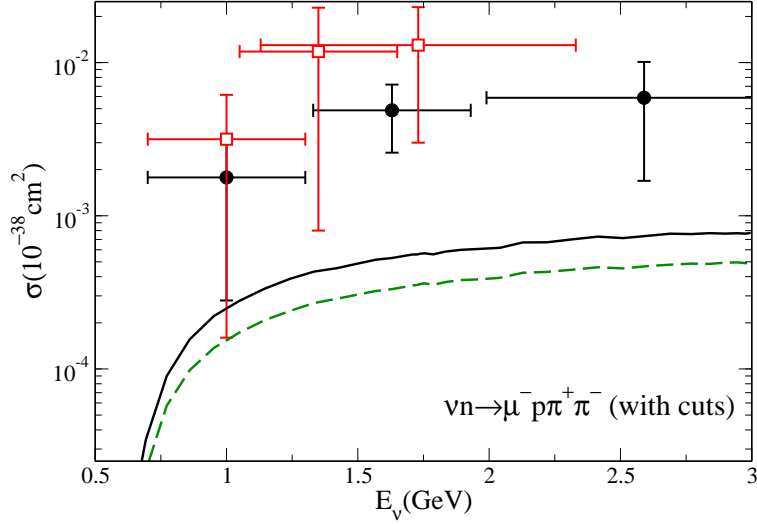


**FIGURE 8.** Cross section for the  $\nu n \rightarrow \mu^- p \pi^+ \pi^-$  with cuts as explained in the text. Dashed line: Background terms. Solid line: Full model with set 1 of nucleon-Roper transition FF. Data are from Ref. [29] (solid circles) and Ref. [35] (open squares).

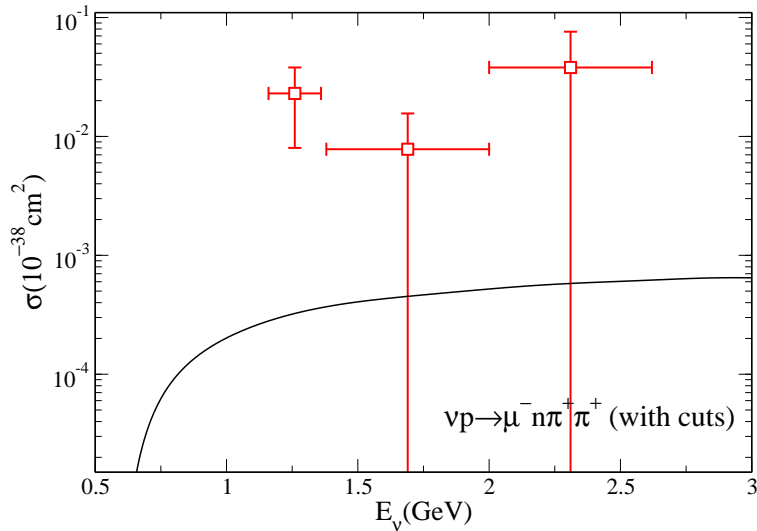


**FIGURE 9.** Cross section for the  $\nu p \rightarrow \mu^- n \pi^+ \pi^+$  with cuts as explained in the text. Note that there are no contributions from the  $N^*(1440)$  resonance to this channel. Data are from Ref. [35].

oscillation experiments some of them which are producing results on cross section measurements. Phenomenological cross section have been used for these processes in modeling the neutrino cross section for validating the Monte Carlo generators for neutrino events. It is desirable that a theoretical calculation of the cross section for these inelastic processes is made available for modelings the neutrino-nucleus cross section in this energy region.

A theoretical understanding of quasielastic hyperon production processes will help us to understand the role of symmetries of weak interaction currents at higher momentum transfer in the quasielastic production of hyperons. In the case of two pion production, there is an urgent need of going beyond the region of threshold production to understand the reaction dynamics of two pion production in weak interaction. Even in the threshold region, there is a need to include other contributions not considered in this work. Experimentally, efforts should be made to observe these reactions in the ongoing experiments looking for neutrino oscillation in the few GeV energy region.

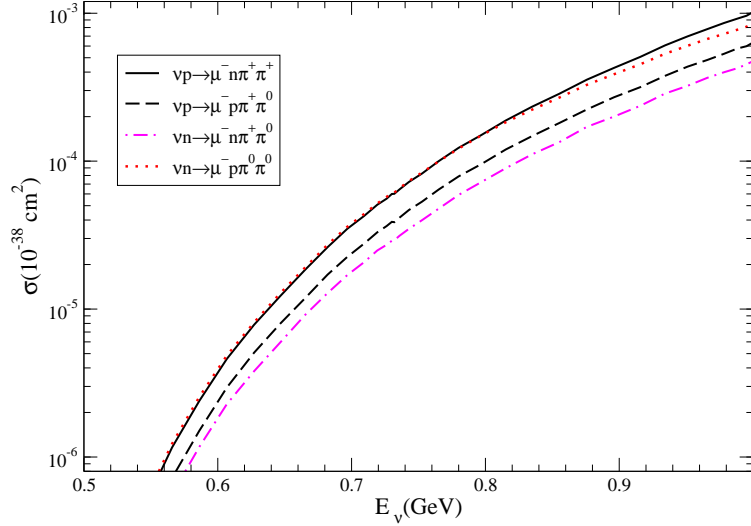


**FIGURE 10.** Cross sections as a function of the neutrino energy. All calculations correspond to the full model with the FF1 set of nucleon-Roper transition form factors.

## ACKNOWLEDGMENTS

One of the authors (S. K. Singh) is thankful to the organizers of the CETUP workshop and specially to Profs. Barbara Szczerbinska, Jan Sobczyk, L. Alvarez-Ruso for the warm hospitality and financial support.

## REFERENCES

1. N. Solomey [Minerva Collaboration], *Nucl. Phys. Proc. Suppl.* **142**, 74 (2005).
2. J. Evans, *Adv.High Energy Phys.* **2013**, 182537 (2013)
3. D. Ayres, et al., [NOvA Collaboration], *FERMILAB-PROPOSAL-0929* (2004).
4. C. Adams, et al., *arXiv:1307.7335* [hep-ex].
5. Abe K *et al.* [T2K Collaboration] *2011 Nucl. Instrum. Meth. A* **659** 106; <http://t2k-experiment.org/>
6. A. Aguilar-Arevalo, et al., *Phys.Rev.Lett.* **98**, 231801 (2007).
7. H. Chen *et al.* [MicroBooNE Collaboration], *FERMILAB-PROPOSAL-0974*.
8. M. Rafi Alam, M. Sajjad Athar, S. Chauhan and S. K. Singh, *Phys. Rev. D* **88** 077301 (2013).
9. M. Rafi Alam, I. R. Simo, M. Sajjad Athar and M. J. Vicente Vacas, *Phys. Rev. D* **82** 033001 (2010).
10. M. Rafi Alam, I. R. Simo, M. Sajjad Athar and M. J. Vicente Vacas, *Phys. Rev. D* **85** 013014 (2012).
11. E. Hernandez, J. Nieves, S. K. Singh, M. Valverde and M. J. Vicente Vacas, *Phys. Rev. D* **77**, 053009 (2008).
12. S. K. Singh and M. J. Vicente Vacas, *Phys. Rev. D* **74** 053009 (2008).
13. J. J. Wu and B. S. Zou, *arXiv:1307.0574* [hep-ph].
14. N. Cabibbo, E. C. Swallow and R. Winston, *Ann. Rev. Nucl. Part. Sci.* **53**, 39 (2003).
15. M. Rafi Alam, M. Sajjad Athar, S. Chauhan and S. K. Singh, *arXiv:1409.2145* [hep-ph].
16. T. Eichten *et al.*, *Phys. Lett. B* **40**, 593 (1972).
17. O. Erriquez *et al.*, *Nucl. Phys. B* **140**, 123 (1978).
18. O. Erriquez *et al.*, *Phys. Lett. B* **70**, 383 (1977).
19. J. Brunner *et al* [SKAT Collaboration] *Z. Phys. C* **45** 551 (1990).
20. G. Fanourakis *et al.*, *Phys. Rev. D* **21**, 562 (1980).
21. K. S. Kuzmin and V. A. Naumov, *Phys. Atom. Nucl.* **72**, 1501 (2009) [*Yad. Fiz.* **72**, 1555 (2009)].
22. J. Finjord and F. Ravndal *Nucl. Phys. B* **106** 228 (1976).
23. L. Fields *et al.* [MINERvA Collaboration], *Phys. Rev. Lett.* **111**, no. 2, 022501 (2013).
24. G. M. Radecky *et al.*, *Phys. Rev. D* **25** (1982) 1161 [Erratum-ibid. D **26** (1982) 3297].
25. T. Kitagaki *et al.*, *Phys. Rev. D* **42** (1990) 1331.
26. S. A. Adjei, D. A. Dicus and V. L. Teplitz, *Phys. Rev. D* **23**, 672 (1981) ; *Phys. Rev. D* **24**, 623 (1981).
27. V. I. Mokeev, V. D. Burkert, T. S. H. Lee, L. Elouadrhiri, G. V. Fedotov and B. S. Ishkhanov, *Phys. Rev. C* **80**, 045212 (2009).
28. V. I. Mokeev *et al.* [CLAS Collaboration], *Phys. Rev. C* **86**, 035203 (2012).
29. T. Kitagaki *et al.*, *Phys. Rev. D* **34** 2554 (1986).

30. E. Hernandez, J. Nieves and M. Valverde, *Phys. Rev. D* **76** 033005 (2007).
31. L. Alvarez-Ruso, E. Oset and E. Hernandez, *Nucl. Phys. A* **633**, 519 (1998).
32. U. Meyer, E. Hernandez and A. J. Buchmann, *Phys. Rev. C* **64**, 035203 (2001).
33. O. Lalakulich, E. A. Paschos and G. Piranishvili, *Phys. Rev. D* **74** 014009 (2006).
34. D. Drechsel, S. S. Kamalov and L. Tiator, *Eur. Phys. J. A* **34**, 69 (2007).
35. D. Day *et al.*, *Phys. Rev. D* **28** 2714 (1983).